Forensic Science International 219 (2012) 76–87

Contents lists available at SciVerse ScienceDirect

Forensic Science International

journal homepage: www.elsevier.com/locate/forsciint

Fundamental studies of bloodstain formation and characteristics

Craig D. Adam *

Faulds Laboratories, Department of Chemical and Forensic Sciences, Keele University, Keele, Staffordshire ST5 5BG, UK

ARTICLE INFO

Article history:
Received 24 August 2011
Received in revised form 20 November 2011
Accepted 12 December 2011
Available online 5 January 2012

Keywords:
Forensic
Bloodstain
Blood dynamics
Blood splash
Blood spatter

ABSTRACT

A detailed understanding of blood droplet impact dynamics and stain formation is an essential prerequisite to the interpretation of both individual bloodstains and spatter patterns. The current literature on theoretical models for the spreading and splashing of liquid drops on surfaces relevant to the forensic context of bloodstain formation has been reviewed. These models have been evaluated for a paper substrate using experimental data obtained as function of droplet size, impact velocity and angle. It is shown that for perpendicular impact there are fairly simple mathematical models for the spreading diameter and the number of scallops or spines formed around the stain though these have quite limited ranges of validity in their basic form. In particular, predictions for the diameter are best for small droplets impacting at high velocity and the number of spines saturates for higher impact velocities. In the case of spreading, a modification to the energy conservation model is found to provide excellent agreement with experimental stain diameters across a wide range of impact velocities. For non-perpendicular impact, the width of stains is found to depend principally on the normal component of impact velocity and may be predicted by an appropriate modification to the expression for the perpendicular case. Limitations in the calculation of impact angle from the stain aspect ratio are identified and a theoretical basis for the prediction of spines around an elliptical stain is proposed. Some key issues for future research are identified which include a systematic, quantitative study of the effect of surface properties on bloodstain formation.

1. Introduction

A detailed understanding of blood dynamics and stain formation is an essential prerequisite to the interpretation of both individual bloodstains and spatter patterns. Within the literature there is a fairly large body of work on both the spreading of liquids following droplet impact and on the splash features that may also be formed in those circumstances. In only a few notable cases has blood been the subject of such study and the forensic context been considered. Consequently there is a need, not only for a review of recent theoretical developments relevant to blood dynamics, but also for a systematic study of bloodstain formation and the application of current theories to model and hence understand the key characteristics of such stains. The work to be described here aims to examine the stains formed following the impact on paper of blood droplets in the millimetre size range and travelling at a variety of angles and velocities. The spreading and splash features are then interpreted following a review of theoretical models and some conclusions drawn as to how such an understanding may benefit the examination of bloodstains in the forensic context.

2. A review of the modelling of spreading and splash

The fundamental problem of explaining and predicting the spread of liquid following perpendicular impact on a smooth horizontal surface has received much attention in the literature; for example, see the review in Ref. [1]. The development of mathematical models has progressed alongside high speed imaging experiments which reveal the mechanisms whereby the impact of a spherical droplet leads to a circular, disc-shaped stain [2]. These show that the impact creates a lamella or boundary layer of liquid in contact with the surface which spreads rapidly in a radial direction while the majority of the droplet remains spherical. This stage is followed by the rim of the lamella swelling as liquid flows outward from the spherical reserve to create a largely-flat, disc-like entity with a swollen rim. The material within the rim may then recede inwards until equilibrium is attained. On surfaces of low wettability this means that the diameter of the final stain is likely to be less than that attained during the spreading phase. On the other hand, where there are surface-specific forces that enhance wetting and are independent of the impact conditions, the final stain diameter can be greater than that generated after the maximum spreading has occurred. Images of these stages are given, for example, in Ref. [2]. Although detail of these processes depends on a number of factors which include the nature of the surface and properties of the liquid, the formation

* Tel.: +44 1782 733854; fax: +44 1782 712378.
E-mail address: c.d.adam@keele.ac.uk.

0379-0738/$ – see front matter © 2011 Elsevier Ireland Ltd. All rights reserved.
doi:10.1016/j.forsciint.2011.12.002

and dynamics of the lamella remains the key to understanding the final size of the stain. It should be acknowledged that, although blood is a non-Newtonian fluid, all studies to date have assumed it behaves as if its viscosity were constant throughout the spreading and splashing process and this approximation has also been adopted in this work.

The models that have been developed to explain these effects are based on fundamental physical processes adapted in some cases with empirical factors so as to best describe observations on a wide variety of liquids and droplet size, impacting over a range of impact velocities. For the present purposes however, attention will focus on those models that predict the behaviour of a low viscosity fluid such as blood impacting as droplets of diameter the order of a millimetre. It is also preferable that the model has the minimum empirical adjustment and that is justified according to some physical origin.

2.1. Modelling spread following perpendicular impact

The spreading of liquid droplets following perpendicular impact appears a simple process but is one that has and continues to be subject to on-going study. Nevertheless, one of the simplest and most successful models is that of Pasandideh-Fard et al. [3] which is based on energy conservation considerations originally proposed by Chandra and Avedisian [2]. This equates the sum of the initial kinetic energy of the falling droplet (KE_1) together with its surface energy (SE_1) to the sum of the final surface energy of the circular stain (SE_2) and the energy dissipated in the viscous deformation of the liquid on spreading (W). Thus from [3]:

$$KE_1 + SE_1 = SE_2 + W$$

$$\frac{1}{2}\left(\frac{\pi\rho d^3}{6}\right)v^2 + \pi\gamma d^2 = \frac{\pi\gamma D^2}{4}(1-\cos\theta_e) + \frac{\pi}{3\sqrt{Re}}\rho v^2 dD^2 \quad (1)$$

In this expression a droplet of diameter d gives rise to a stain of maximum spreading diameter D following impact at velocity v. The relevant properties of the liquid are the density ρ, the viscosity η and the surface tension γ while the equilibrium contact angle of the liquid with the surface is given by θ_e. The dimensionless Reynolds number Re relating some of these quantities is given by:

$$Re = \frac{\rho v d}{\eta}$$

The last term in Eq. (1) is both the most important and the most difficult to determine so approximations have to be made, in particular with respect to the thickness of the expanding lamella. It is this aspect that authors have differed in their approaches (e.g. [2], [3]). The final result is often expressed as the ratio β of the maximum spreading diameter D to that of the droplet d. Thus from Eq. (1) we get:

$$\beta = \frac{D}{d} = \left(\frac{We + 12}{3(1-\cos\theta_e) + 4WeRe^{-1/2}}\right)^{1/2} \quad (2)$$

Here, the dimensionless Weber number We is defined as:

$$We = \frac{\rho v^2 d}{\gamma}$$

Since the main mechanism for the spread of larger droplets impacting at higher velocities is conversion of kinetic energy to viscous deformation in forming the stain, both surface energy terms may be neglected in these circumstances to give a simplified version of Eq. (2) [3]:

$$\beta = \frac{D}{d} = \frac{1}{2}Re^{1/4} \quad (3)$$

It should be noted that while Eq. (2) implies that stain size reduces to the realistic scenario of a constant value as the impact velocity deceases to zero, this is not the case for Eq. (3), implying that is has a lower limit on its validity. By viewing Eq. (3) as a limiting form of Eq. (2) shows that while surface tension has some significance in defining the spread of a bloodstain at low impact velocities, this factor is of little relevance at the higher velocities typical of most stains found in casework. In the form of Eq. (3), the model has been applied previously [4] to explain the diameters of bloodstains formed on a variety of non-porous surfaces. The variation in stain size ascribed to differences in surface roughness was small but distinct. Nevertheless in all cases this simple model gave approximate agreement with experimental data obtained over a limited number and range of impact velocities though no correction for air resistance was applied. By including an empirical correction factor of 1.11 the model was adjusted to the mean behaviour across all four surfaces in this work. However, as the comparison between theory and experiment was not displayed using the linear relationship of Eq. (3), systematic differences between the model and the data were not discussed.

This energy conservation model (Eq. (2)) has been compared against other models [5] and refined further to provide an albeit small correction for the fact that the spreading lamella is not strictly cylindrical and that consequently the thickness of the rim needed to be revised to more correctly model the surface energy of the stain. The equilibrium contact angle θ_e was also replaced by the advancing contact angle θ_a to provide an additional, minor correction. This is of little significance except at very low impact velocities and in this work the value of the equilibrium contact angle has been used where necessary. The resulting energy balance equation may be now written as:

$$(We + 12)\beta = 8 + \beta^3\left(3(1-\cos\theta_a) + \frac{4}{\sqrt{Re}}We\right) \quad (4)$$

More recently [6] further experimental measurements have validated this model against liquids with a range of viscosities and the importance of this correction verified. Although both these modifications have greatest impact at lower impact velocities, their relevance to the spreading of bloodstains has not yet been assessed. The models represented by Eqs. (2)–(4) are described graphically for blood in Fig. 1. The abscissa is taken as the non-

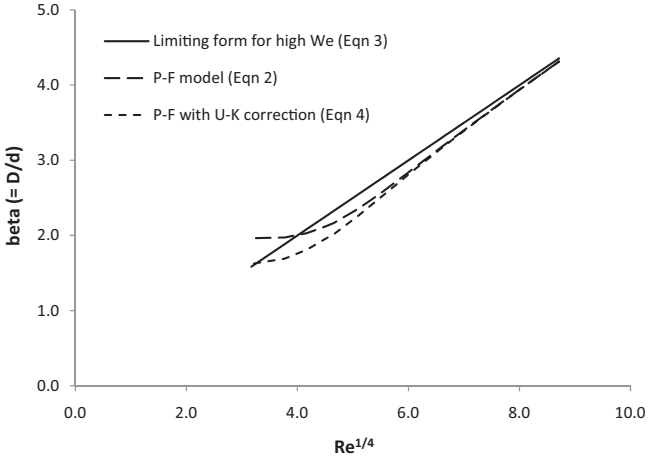

Fig. 1. Basic models for the spreading diameter of a circular blood-stain.

dimensional parameter $Re^{1/4}$ as this presents Eq. (3) in a linear fashion and the other two as deviations from that linearity. The range of this graph goes from a vanishingly small impact velocity to that approaching a 2 m drop under gravity. The more parameterised models (Eqs. (2) and (4)) imply that stains should have sizes less than that predicted by Eq. (3) and that the relationship between β and $Re^{1/4}$ deviates from linearity except at the highest velocities.

It should be noted that there are other models for spreading that have been successfully validated by experimental measurement; some of these are reviewed in Ref. [6]. Many do depend however on constants which are found empirically. The models shown in Fig. 1 have both the advantage of mathematical simplicity and limited empirical adjustment.

2.2. Modelling splash following perpendicular impact

The generic term *splash* is usually applied to those features around the circumference of a stain where thin fingers or spines of liquid are thrown outward beyond the rim to give a crown-like appearance sometimes termed corona splash. In general splash features are associated with higher impact velocities. However at lower speeds the circumference may assume a wave-like appearance (often termed scalloped) similar to splash but where no liquid is ejected from the main body of the stain. Interestingly, in reviewing previously published work it appears that this distinction does not seem to have been addressed as relevant to theoretical models of splashing. Finally, at the lowest impact velocities stains from perpendicular impact have a smooth circular rim. The condition that marks the transition to splash features on the stain may be mathematically defined and is termed the splash threshold [7]. This is based on empirical data which show correlation with surface roughness measurements so would not necessarily transfer across to other surface characteristics that might suppress splashing such as elasticity.

The origin of both spine and scallop features (Fig. 2) has generally assumed to be due to Rayleigh–Taylor instability in the fluid flow due to the rapid deceleration of the liquid on hitting the lower density air around the stain [8]. This causes wave-like undulations around the circumference with a wavelength dependant on the deceleration, surface tension and density of the liquid. Hence the number of scallops or spines observed will depend on how many wavelengths fit around the rim of a particular diameter of stain. Such arguments were presented [9] to show that these may be predicted using:

$$N = \sqrt{\frac{WeRe^{1/2}}{48}} \tag{5}$$

The form of this equation appears to support – through the factor $WeRe^{1/2}$ – the much earlier empirical result [7] which attempted to predict whether splashing will take place for a particular liquid impacting on a surface under specific conditions. Here the splashing threshold is given by [7]:

$$WeRe^{1/2} > K \tag{6}$$

where K is characteristic of a particular surface and has been shown to correlate well with roughness. Note that strictly Ref. [7] gives the square of this expression (We^2Re) as the threshold and indeed some authors have used the square root as the criterion! All these are equivalent though the absolute values of K will differ in each case. The combination of these two Eqs. (5) and (6) appears to suggest that for a particular surface there will be a minimum number of spines observable around any stain. Despite the form of Eq. (5), it has been shown [10] that better agreement with

Fig. 2. Examples of scallop (top) and spine (bottom) features on bloodstains arising from a 4.21 mm diameter droplet impacting perpendicularly on to paper.

experimental data is given by:

$$N = 1.14We^{1/2} \tag{7}$$

where the factor of 1.14 was empirically derived to produce the best agreement with experimental results. Splash features around bloodstains have been shown [4] to follow Eq. (7) to some extent with the factor further modified to be more or less unity. However deviations from this model could not be identified as the data were not presented in a linear fashion. In a subsequent publication [11] it was shown how measurements on stain size interpreted using Eq. (3) could be combined with this interpretation of splash features (Eq. (7)) to derive estimates for both the impact velocity and size of a blood droplet. This provides a potentially powerful tool in bloodstain interpretation.

The implication of these results is that until the impact conditions – principally a sufficiently high velocity – satisfy Eq. (6), true splash will not be observed. However, at lower impact speeds, scallops or a smooth edge will be the outcome. Whenever such features are observed, their number is best predicted by Eq. (7) [10]. More recently [12] it has been suggested that there are two possible mechanisms for splash. So-called corona splash is driven by the impact on the air around the stain and predominates on smooth surfaces. However, the dependence of this mechanism on air pressure throws doubt on the validity of the Rayleigh–Taylor mechanism which is driven by the density difference between the liquid and the surrounding air, in favour of the Kelvin–Helmholtz mechanism which depends on corresponding velocity difference.

On rougher surfaces so-called prompt splash may result which depends on the texture of the surface. In general both mechanisms are likely to be present to varying degrees and this may reduce the transferability of Eq. (7) across a wide range of surfaces.

Finally, brief attention will be given to the effect of the characteristics and properties of the surface itself on spreading and splashing behaviour. In addition to roughness which has been the subject of most attention in the literature, the elasticity, wettability and porosity of the surface are likely to be significant factors in cases where the surface is not a relatively smooth, rigid and non-porous substrate [6].

Although it does not appear to have a very significant effect on spreading [1,4], surface roughness is recognised as a factor in determining the splashing threshold. This is particularly the case for low levels of roughness where an increase in roughness reduces the splashing threshold and thereby promotes splashing. Conversely a highly polished surface will suppress such phenomena by increasing the threshold [1]. These qualitative links between surface texture and splash features have long been recognised within the forensic context. Porosity in the surface will encourage dissipation of energy through the removal of liquid from the stain. The elasticity of the surface has been found to affect the splashing threshold [13]. While a rigid surface has a fairly low threshold this increases as the elasticity increases since more of the energy on impact is taken up as elastic energy in the surface.

2.3. Non-perpendicular impact

In contrast to perpendicular impact, studies of the dynamics of liquid droplets impacting on an inclined surface are far fewer in number and consequently fundamental aspects of the formation of stain characteristics are more poorly understood. Bloodstains resulting from angular impact are considerably more complex in appearance than those just discussed. They show distinct variation in shape, size and splash features with respect to impact conditions (Fig. 3).

It was shown some time ago that the basic shape of the stain is predominantly elliptical though this may show some elongation in the forward direction. Measurement of the axial ratio (W/L) leads to a good estimate of the impact angle θ, conventionally measured from the surface, according to the accepted formula:

$$\sin\theta = \frac{W}{L} \tag{8}$$

A commentary on this early work has recently been published [14]. Although it appears that this formula works satisfactorily in practice and is justified to some extent on geometric grounds, surprisingly there is no published detailed analysis of its reliability across a full angular and impact velocity range. A semi-quantitative study using high speed photography discussed some of the characteristics of such stains and in particular has verified that impact on an inclined surface produces similar stain features to those found following perpendicular impact onto a moving substrate [15].

Most interest in recent years has centred around the splashing of droplets on inclined surfaces often using moving belts or rotating cylinders to generate the necessary tangential velocity component. Once again high speed photography has been used to investigate the mechanisms underpinning these phenomena. In particular, it has been shown that the normal component v_n ($v_n = v\sin\theta$) of impact velocity and hence the corresponding Re_n and We_n numbers, determine the formation of splash features [16,17]. Hence, following the work of Ref. [10], the basis of an expression for the number of spines will be:

$$N = 1.14We_n^{1/2} = 1.14We^{1/2}\sin\theta \tag{9}$$

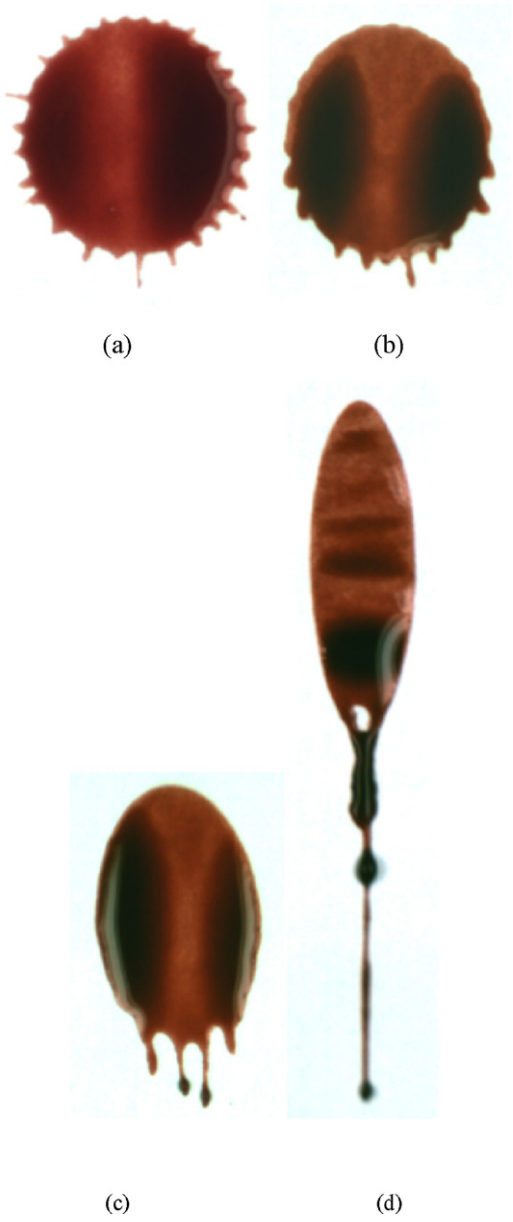

Fig. 3. Examples of stains following non-perpendicular impact from a 0.8 m drop height: (a) $\theta = 80^\circ$; (b) $\theta = 60^\circ$; (c) $\theta = 40^\circ$; and (d) $\theta = 20^\circ$.

This shows that as the impact angle is decreased the maximum number of spines produced will be reduced. It also appears reasonable that the transverse spreading of the stain which should be largely unaffected by the impact angle also depends on v_n and hence the elliptical stain width W would be given by modifying Eqs. (1)–(3) appropriately, for example:

$$W = \frac{d}{2}Re_n^{1/4} = \frac{d}{2}Re^{1/4}\sin^{1/4}\theta \tag{10}$$

Further, the tangential component v_t of velocity ($v_t = v\cos\theta$) is responsible for either enhancing or suppressing splash around the rim of the elliptical stain thereby causing the observed asymmetry in splashing [18]. An expression has been derived [17] that defines the splashing thresholds in both the forward and backward directions of a stain formed on impact. Since the ratio of the tangential and normal velocity components is given by:

$$\frac{v_t}{v_n} = \operatorname{cotan}\theta$$

this expression may be written as:

$$We_n Re_n^{1/2}[1 \pm kRe_n^{-1/2}\,\mathrm{cotan}\,\theta]^2 > K \quad (11)$$

The constant k is of order one while K depends on the surface roughness. It is clear that Eq. (6) is a special case of this result for perpendicular impact. When the negative sign is taken the splashing threshold is reduced as the tangential velocity component suppresses splash while for the positive sign enhancement occurs and the threshold is raised. This result explains why splash features are enhanced in the forward direction and increasingly suppressed in the backward direction as the impact angle is reduced from 90° (Fig. 3). Around the circumference of the stain the component of v_t acting in the direction of spine formation will change thereby generating a gradual movement of the threshold for the onset of splash from the back direction round the rim towards the forward direction as the impact angle decreases (see Fig. 3). In addition there will be fewer spines in total as the angle is reduced since the normal component of impact velocity is decreasing (Eq. (9)).

It is clear from geometrical considerations that the impact point of the droplet on an inclined surface is not in the centre of the consequent elliptical stain; rather it lies towards the back side of the stain and increasingly so as the incident angle decreases [16]. Since this is source of the rapidly moving lamella which is responsible for the characteristics if the stain, it implies that any spines should be directed towards this point. The spread of the lamella from the contact point is asymmetric as the difference in the velocities of the front and back edges of the lamella increases as the impact angle decreases. When the radial velocity of the back edge tends to zero it has reached its maximum extent [16].

In the only related study in the context of blood [19], empirical relationships were derived for the area of the elliptical stain and the number of spines in terms of the impact angle. These were seen as a general case of the equations used in Ref. [4] for the specific instance of perpendicular impact on a surface. More recently [20] experimental data from the angular impact of water droplets on a PVC surface was used to validate the application of Eq. (3) (for $We < 1000$) to relate the area of the elliptical stain to the incident droplet diameter. The implication of the outcome of this work is that the area of a stain depends only on the initial droplet diameter and the impact velocity, not on the impact angle. Nevertheless it was also indicated that, for low impact angles ($\theta < 21°$), the tangential velocity component tends to override any transverse spreading of the droplet [20].

There is one splash feature which is only observed following non-perpendicular impact. This is a single cast-off feature. Since this always appears in the forward direction, it will be termed a cast-forward feature for clarity (see Fig. 3(d)). This may vary in appearance from a small relatively wide protuberance to a very long slender strand which may display wave cast-off structure [15]. It originates from a small amount of the liquid not being retained within the stain but continuing to move forward across the surface on impact. This appears to not have received any theoretical attention in the literature but should not be regarded as a spine but as a quite separate splash feature.

3. Experimental methods and materials

The basic experimental technique for producing bloodstains under specified impact conditions is fairly straightforward though care needs to be taken at various points to ensure the reproducibility of results. Human blood was obtained as a single sachet from the UK National Blood Transfusion Service and either used when fresh or after freezing and subsequent overnight defrosting in a refrigerator. Appropriate safety precautions were taken throughout its use. All samples were agitated and brought to room temperature before use. Each sample was used for only a short period before a fresh amount of blood was taken from the refrigerator. These procedures were found to produce consistent results. Paper was chosen as a model substrate due to its uniform surface quality which has a low roughness and absorption, yet is not non-porous. Surface dependant effects were thereby minimised during the formation of stains and for this substrate it was considered justifiable to take the final stain diameter as the maximum spreading diameter D.

A glass separating funnel fitted with a tap acted as a reservoir for the blood and was secured to a Kaiser *rePro* photographic camera (copy) stand that allowed smooth variation in drop height over a wide range. Plastic nozzles were fitted to the reservoir as required to provide appropriately sized droplets. Droplets could be produced reliably by careful control of the tap. All stains were produced on standard photocopy paper taped to rigid cutting-mats which could be easily moved across to a separate camera stand for immediate imaging. The cutting-mats were either placed on the base of the camera stand or on an adjustable inclined plane to generate the required angular impact. Imaging was carried out using a Motic digital camera and images were analysed with Motic Images Plus 2.0 imaging and analysis software. Calibration was achieved by an x–y scale placed alongside the stains prior to imaging. Circular stain diameters and the length and breadth of elliptical stains were measured by manual fitting of either a circular or elliptical outline to each stain displayed on the computer screen. Splash features were examined manually in a similar fashion. For perpendicular impact a second method was used for this latter measurement based on measuring the angle subtended by a group of well-formed and regularly spaced scallops or spines around the circumference of the stain and scaling that number up to the full circumference. Due to axial symmetry these features should be regularly spaced and only disrupted by minor perturbations during impact. By ignoring those parts of the stain outline and using only a sequence of unperturbed spines and scallops it was found that there was less scatter in the final data. Angles were measured using an appropriate tool in the Motic software.

Droplet volumes were obtained gravimetrically as an average of fifty droplets, assuming a typical density for blood of 1060 kg m^{-3} then converted to diameters by assuming a spherical shape. Although oscillation of the droplet may take place when it is released [21], these die away quite rapidly [7] though the decay rate is slower for larger droplets. For blood droplets in the size range used in this work it has been shown that oscillations are not detectable after a fall of 0.4 m [21]. Other studies using high-speed photography has shown that, on impact, droplets have a spherical shape to a good degree of approximation [22]. For the perpendicular impact experiments, three droplet sizes were used and for each around 35 separate measurements made across the range of drop heights from 0.01 to 1.90 m. Angular impact experiments were made for one droplet size only (4.21 mm diameter) at 10° intervals from 90° down to 20° with around 12 separate drop heights at each angle over the same height range. The heights were selected to ensure that the impact velocity range was explored at uniform intervals. In all cases five repeat stains were produced and an average for each measurement calculated. The approximate equilibrium contact angle for a blood droplet on photocopier paper was measured using the sessile drop method and yielded a value of 82° ± 3°.

It was essential to obtain accurate measurement of impact velocity so a separate set of calibration experiments was carried out using a set of optical gates linked to a Pasco measurement system. This enabled the impact velocity and the time to impact to be obtained over an appropriate range of drop heights for all three droplet sizes. To achieve the desired flexibility when analysing the later data sets, these results were used to fit kinematic equations incorporating air resistance, which were subsequently used to obtain the correct impact velocity for any specified drop height. It was found that the effects of air resistance were best modelled by a term quadratic in velocity typical of turbulent flow. The velocity v and time t data were used to determine the air resistance coefficient, expressed as the equivalent terminal velocity v_T for a particular droplet size, using [23]:

$$v(t) = v_T \tanh\left(\frac{gt}{v_T}\right) \quad (12)$$

To determine the impact velocity for any particular height, the time to impact was calculated from the drop height using:

$$y(t) = \frac{v_T^2}{g} \ln\left(\cosh\left(\frac{gt}{v_T}\right)\right) \quad (13)$$

The time was then used to calculate the impact velocity using Eq. (12). Fig. 4 shows the velocity versus drop height characteristics for each of the three blood droplets sizes.

All measurements were stored within Excel spreadsheets where all the data processing and analysis was carried out. Finally, values for the viscosity (η = 0.0044 Pa s) [4] and surface tension (γ = 0.062 N m^{-1}) [24,25] of human blood were taken from the literature. Although the precise values adopted are not crucial to the detailed interpretation of the results, it is pertinent to comment on the viscosity in particular. As a non-Newtonian fluid the viscosity of blood is shear-dependent, reducing in magnitude as the shear is increased. The shearing forces experienced during the spreading of the stain are unknown and so whatever value is adopted will be an estimate with some associated uncertainty. The average viscosity of 0.0044 Pa s quoted in Ref. [4] is identical to the mean value found in a separate study [26] across a large sample of healthy adults measured under conditions of moderate shear. The standard deviation across the sample given for this study was 0.0006 Pa s which implies a relative standard deviation (RSD) of 14%.

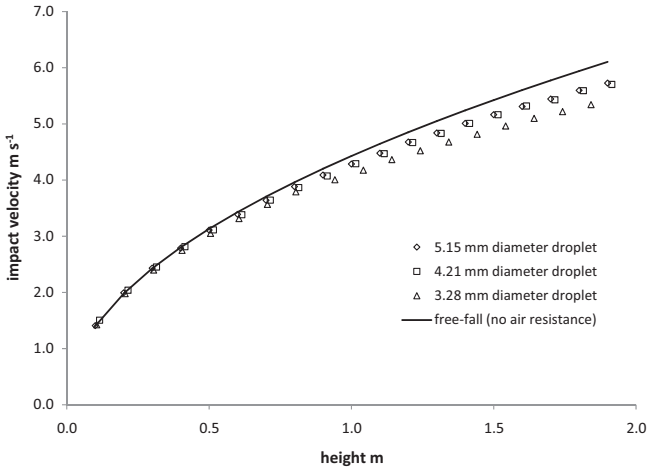

Fig. 4. Velocity versus drop height for the three blood droplet sizes.

It is reasonable to suppose that, as the blood used in this present work came from the UK Blood Transfusion Service, it originated from a healthy adult, providing justification for using this particular value here. Finally, as the stain diameter is a function of the viscosity to the power of a quarter (Eq. (3)), a RSD of 14% would give a consequent RSD in D, arising from this uncertainty in the viscosity, of around 3.5%.

4. Results

The stains were found mostly to be highly reproducible. Standard errors expressed as a percentage of the measurement were in a range up to 1% with an average of 0.6% for measurements of stain diameters on perpendicular impact and nearer to an average of 0.8% for widths and lengths on non-perpendicular impact. In the latter case the uncertainty was at the higher end of this range for the more oblique impact results. In counting scallops and spines the absolute standard error was around ± 1 for perpendicular impact. Uncertainty was higher for non-perpendicular impact as the magnitude of the features could be very small and harder to define.

4.1. Perpendicular impact

Initially, to assess the spreading behaviour of all three droplet sizes, the circular stain diameter D has been plotted against $v^{1/4}$, and compared with the basic theoretical predictions from Eq. (3). This is presented in Fig. 5.

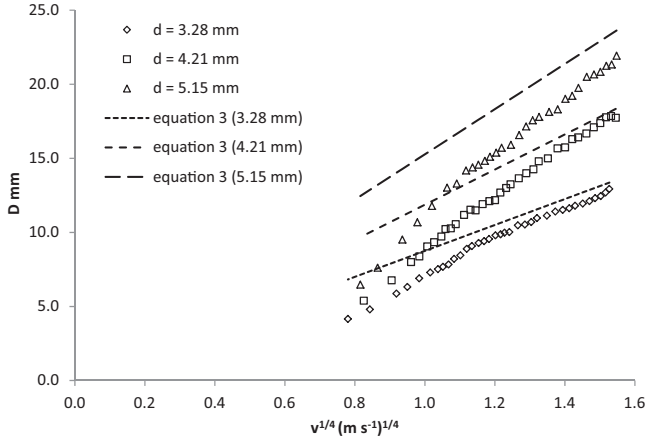

Fig. 5. Experimental stain diameters as a function of $v^{1/4}$ for all three droplet sizes.

In all cases the data appear to follow two separate linear trends – one for lower velocities and the other for higher velocities. All tend towards following the line indicated by the basic model (Eq. (3)) only at the very highest velocities with the data for the smallest droplet showing the best agreement over the largest range while that of the largest droplet falls short of the model over almost all the range of these measurements. Overall the basic model falls far short in following the trends both in gradient and intercept of all three sets of experimental data. For all three sets of measurements there is a distinct bend in the graph at the point where the two linear trends meet. In order to explore this in more detail a second graph was produced. This time each stain was allocated one of the three categories: no splash; scalloped; spines. These designations were made subjectively. The criterion invoked to distinguish between the last two was the nature of the curvature at the features. For scallops there should be a clear convex outline while for spines this should have developed into a discontinuity or point from which liquid may splash outward. These data are given in Fig. 6.

Inspection of Fig. 6 reveals that the bend in the data appears to occur at the point where scallop features start to appear. This means that for stains exhibiting either scallops or spines, Eq. (3) appears to form the basis of an appropriate model whereas for stains with no features around the circumference this model does not provide a fit to these data.

Bearing in mind that Eq. (6) is believed to define the splashing threshold, the values of the two characteristic quantities $WeRe^{1/2}$ and We have been determined from these data and are given in Table 1. These appear to show that a value of $K \sim 26{,}500$ is appropriate for the formation of spines around bloodstains on paper while the onset of scallops is governed rather by the We number alone with a value of 240 being suggested here. It is worth noting that the spine threshold could arguably be given alternatively by $We \sim 560$ on the basis of these data.

As is suggested by Eq. (7), the number of spines or scallops around each stain plotted against $We^{1/2}$ should result in a straight line graph that is independent of droplet size. Examination of Fig. 7 shows that this appears to be true for $We^{1/2} < 35$ or so. However, for larger values, the data veers away from this trend to follow a path of lower gradient. For comparison the line satisfying $N = We^{1/2}$ is included in this graph and appears to follow the trend of these data extremely well suggesting that in this case the empirical coefficient in Eq. (7) should be around unity, as was found previously for blood [4]. It was noted that the point at which the data deviates from this trend does not correspond particularly to the transition from scallops to spines so its origin seems unconnected with these characteristics of the stain. The implication is that as the impact velocity (and hence We) increases further the number of spines appears to saturate. This hypothesis has been previously suggested though not experimentally verified [10] and appears to be supported by Fig. 8 which shows the length occupied by a spine around the circumference of the stain as a function of $We^{1/2}$. For lower impact speeds (and $We^{1/2}$) this quantity increases quite rapidly and corresponds to the linear section of Fig. 7. However for larger values of $We^{1/2}$ where Fig. 7 deviates from the $We^{1/2}$ law, the length per spine tends to a constant value in the range 1.3–1.6 mm with some small differences in that limit dependant on the droplet size.

It was also observed from these data that the number of spines occurring at the splash threshold is independent of droplet size and equal to 20–22 across all three cases. This is in fair agreement with the prediction of Eq. (5):

$$N_{\min} = \sqrt{\frac{26,500}{48}} \approx 23.5$$

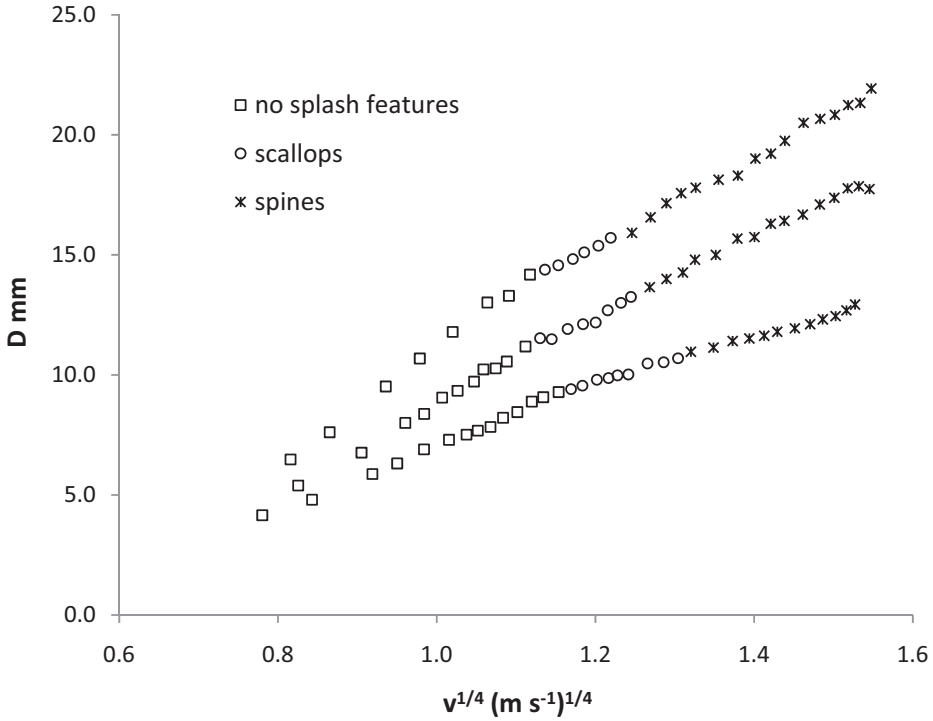

Fig. 6. Experimental stain diameters as a function of $v^{1/4}$ categorised according to the presence of splash features.

In contrast, the minimum number of scallops appeared to increase slightly with increasing droplet size, from a value of 12 to around 15 for the largest droplet. In summary, while the form of Eq. (7) is appropriate to predict both the number of scallop and spine features, the threshold criterion (Eq. (6)) appears valid for spine formation specifically.

4.2. Non-perpendicular impact

Firstly, the hypothesis that the transverse spreading of the stain is determined by the perpendicular component of the impact velocity (Eq. (10)) was examined by plotting the stain width W against $v_n^{1/4}$ for each impact angle to produce graphs analogous to Fig. 5. These are shown together in Fig. 9. The prediction of Eq. (10) is provided for comparison.

It is clear that for impact angles from 90° down to 40° the dependency is identical and follows the trend set by perpendicular impact. This is an important result in determining the principal factor responsible for the width of an elliptical stain. However for the lowest impact angles of 30° and 20° there is only agreement for the very lowest velocities with the stain widths increasing at a slightly lower rate than predicted over most of the range examined here. This suggests that when the tangential velocity component v_t is high it may override the effect of v_n to some extent as was previously suggested [20].

Next the validity of Eq. (8) for the calculation of impact angle from the stain dimensions was investigated, particularly as a function of impact speed. These results are given in Fig. 10. The horizontal dotted lines define the impact angles set in each experiment. These graphs show some quite subtle variations across both the speed and the impact angle ranges examined here. In general the accepted formula (Eq. (8)) will underestimate and rarely overestimate the impact angle. It appears to be most reliable at impact speeds above ~3 ms^{-1} – equivalent to drop heights above ~0.5 m – and for angles below ~60°–70°. For angles around 80° and for low impact speeds the formula appears to underestimate the angle by up to 7° or so. This result is important as it suggests there are systematic as well as random uncertainties in the use of Eq. (8) in the interpretation of blood spatter patterns.

Initial interpretation of the features around elliptical stains may be made qualitatively by assessing the type of feature at the front and back edges of the stain as a function of the perpendicular and

Table 1
Experimental threshold values for scallops and spines.

Droplet d (mm)	We		$WeRe^{1/2}$	
	Scallops	Spines	Scallops	Spines
3.38	224	593	7860	26,499
4.21	213	536	7780	24,656
5.15	272	568	11,109	27,909

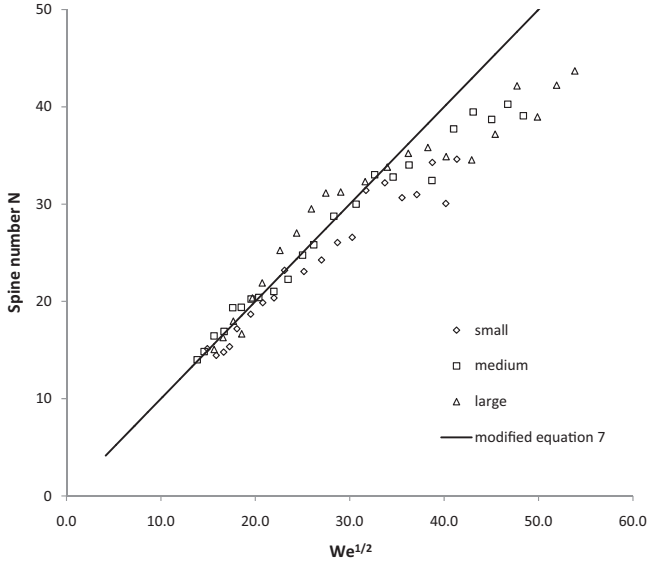

Fig. 7. Spine/scallop number against $We^{1/2}$ for all droplet sizes.

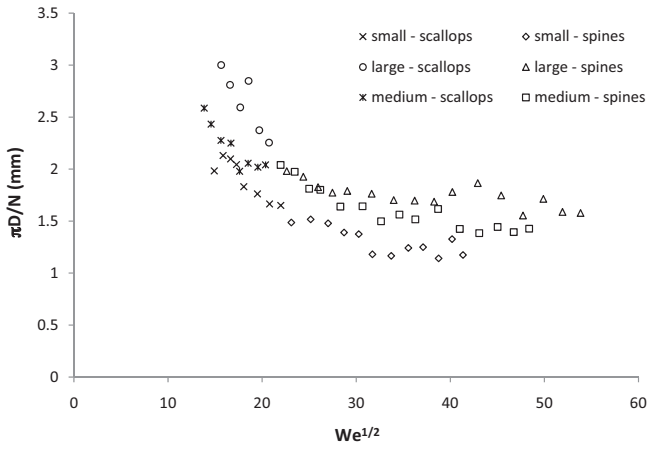

Fig. 8. Length per spine around the circumference of stains as a function of $We^{1/2}$.

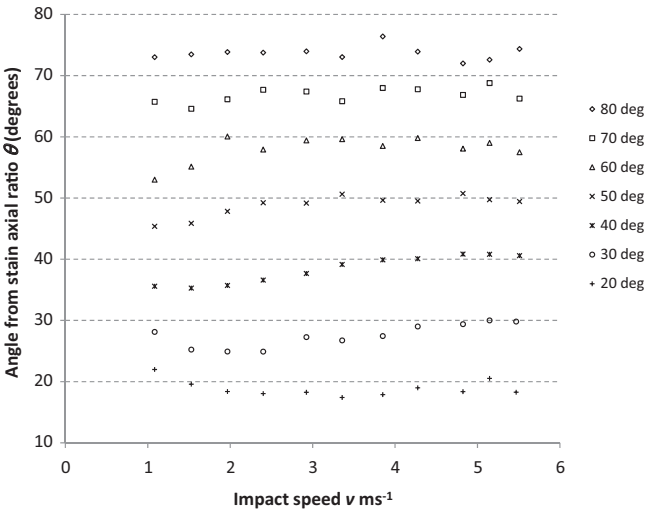

Fig. 10. Comparison of the impact angle calculated from the stain axial ratio with those set in each experiment, as a function of impact speed.

tangential velocity components to produce a "map" of scallops, spines and cast-forward (Fig. 11). Features at the forward edge of the stain are on the right while those at the back are on the left of this figure. A radial line outward from the origin corresponds to a constant impact angle. A key outcome of this is that the cast-forward feature occurs only when the impact angle is below $\sim 45^\circ$ (implying that $v_t > v_n$) and at lower impact velocities.

Next the total number of scallops and spines around the elliptical stains may be interpreted by comparing the total number of such features with the basic theoretical prediction of Eq. (9). These data are displayed in Fig. 12 where the solid line represents Eq. (9) evaluated for perpendicular impact with the constant factor amended to unity following the interpretation in Fig. 7.

This shows that as expected the data for 90° impact agrees with that displayed in Fig. 7 while there is a systematic decrease in the total number of spines as the impact angle decreases down to 40° below which no spines are formed for this range of impact speeds. For each angle however the variation with $We^{1/2}$ remains approximately linear. This behaviour is, of course, expected as the splashing threshold will decrease as θ decreases at a rate given by the angular factor contained in $We^n Re_n^{1/2}$. The rate at which spines are suppressed from the stain will show a similar angular dependence though the detail of this depends on the effect of the tangential component of velocity as it acts around the stain circumference as indicated specifically for the forward and backward extremes in Eq. (11). Nevertheless the general direction of the trend will be given by the factor in front of the bracket in

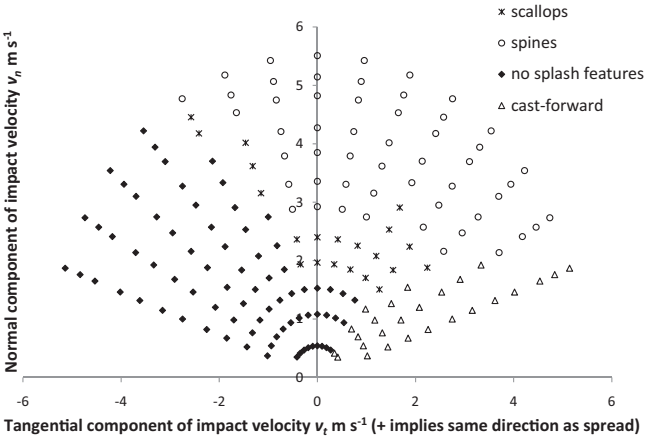

Fig. 11. Velocity map of splash features around elliptical stains.

Eq. (11) and hence the change in the proportion of spines seen will be given approximately by:

$$\frac{We_n Re_n^{1/2}}{WeRe^{1/2}} = \sin^{5/2}\theta$$

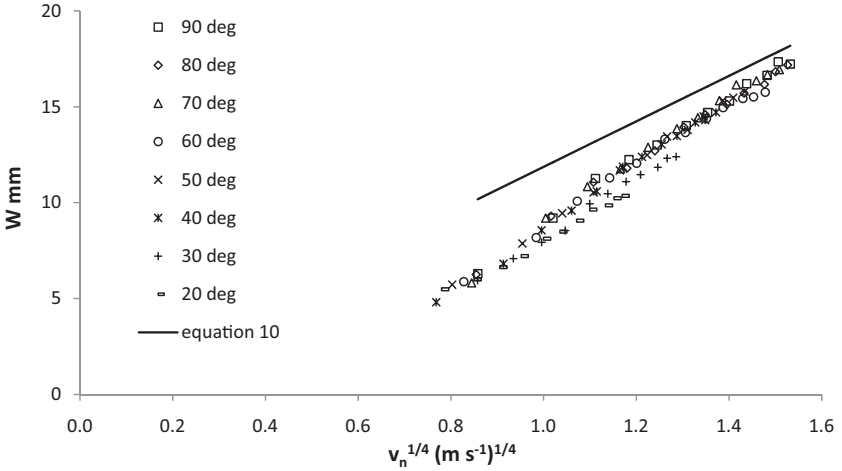

Fig. 9. The transverse width of stains W as a function of $v_n^{1/4}$.

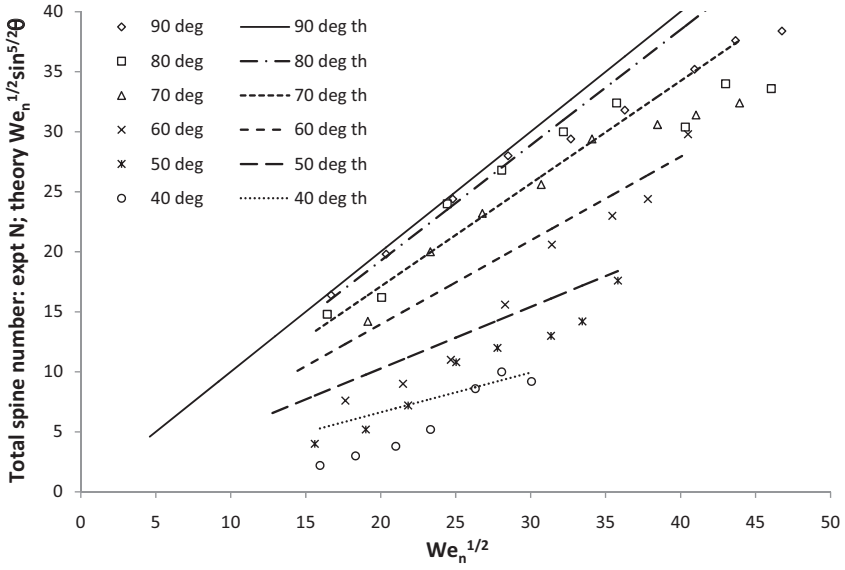

Fig. 12. Variation of total spine number versus theoretical predictions for elliptical stains.

This implies that a correction may be applied to the form of Eq. (9) to give:

$$N \sim We_n^{1/2} \sin^{5/2}\theta = We^{1/2} \sin^{7/2}\theta \tag{14}$$

This expression is represented for each of the impact angles in the form of dashed lines in Fig. 12. While these do not provide a full explanation of the experimental measurements it is clear that they do explain the general variation with angle particularly for higher numbers of spines. These predictions should define to some extent the maximum number of spines and this is borne out by Fig. 12. It is worth noting that the form of Eq. (14) is close to the empirical dependency on $\sin^3\theta$ for angular impact data found previously [19]. Indeed the multiplicative correction factor needed to bring Eq. (14) into best-fit agreement with these data is found to be 0.88 which is similar to the factor of 0.76 found by these authors for their system.

The effect of the tangential velocity component on splash threshold defined by Eq. (11) may be evaluated against the experimental measurements by plotting $WeRe^{1/2}/K$ against cotan $\theta/Re^{1/2}$. This relationship is shown in Fig. 13 where each point represents the presence or absence of splash features on a stain. The threshold itself is defined by a solid line where the arbitrary constant k has been adjusted to best fit the data (k = 6.5). It is apparent that in the forward direction – representing the front of the elliptical stain – this model predicts the threshold from non-splash to splash features quite well. However, in the backward direction it is far less successful, particularly as the magnitude of the tangential component increases. In this region the suppression of splash around the back of the stain appears to occur more readily than is suggested by Eq. (11). However it can be difficult to assess the presence of closely-spaced yet very small spines around the back edge of some of these stains and this may have led in a few cases to the conclusion of suppression when it may have not in fact have occurred.

In summary, these investigations have shown that the width of the elliptical stain depends on impact conditions in the same way (Eq. (10)) as does the diameter of a circular stain, except for low

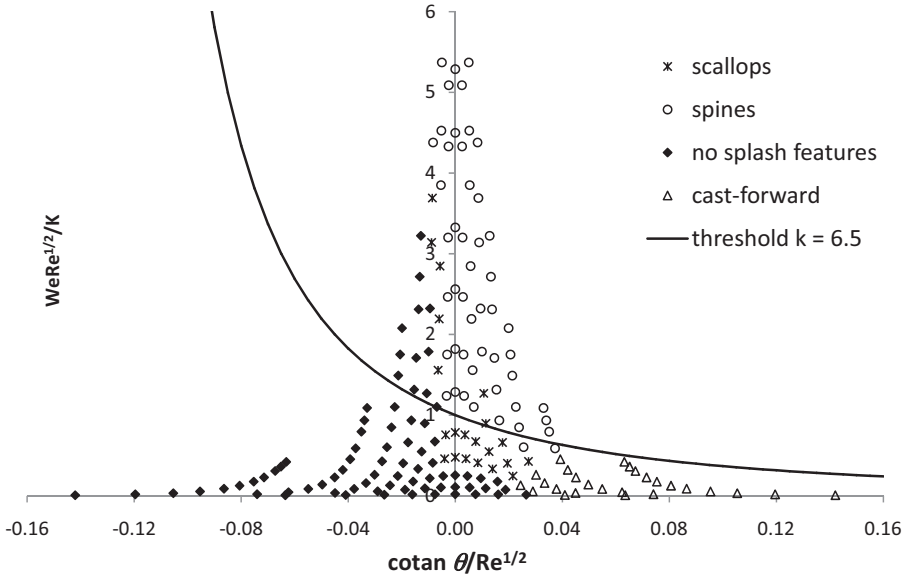

Fig. 13. The interpretation of the splashing threshold for angular impact stains.

impact angles of ~30° or less when it overestimates the magnitude. The conventional formula for calculating impact angle from the aspect ratio of a stain (Eq. (8)) will generally underestimate and rarely over-estimate that angle. It works best for higher impact speeds and for impact angles below ~70°. The formation of spines around an elliptical stain is principally determined by the impact point and the perpendicular component of velocity. However since the effect of the splash threshold changes with impact angle and the tangential component of the velocity may act to suppress spine formation, fewer spines are observed than predicted by Eq. (9). It has been shown that the consequent inclusion of a trigonometric factor in this expression, based on the splashing threshold, provides a theoretical basis to support previous empirical justification [19] relating spine number to impact conditions for such bloodstains.

5. Discussion

5.1. Spreading behaviour for perpendicular impact

The results for perpendicular impact have revealed the following points as far as bloodstain formation on paper is concerned. The model for stain diameter expressed as Eq. (3) most accurately describes stains formed from smaller droplets travelling at higher speeds. For larger droplets and lower impact velocities this expression overestimates diameters. This is not out of line with previous work as most studies have been on droplets at the lower end or below the size range investigated here (Table 2).

However the fact that all experimental stain diameters are lower than the size predicted by an energy balance model suggests that some energy is being dissipated in a manner not already accounted for. Such differences cannot be explained simply by incorporating some constant multiplicative correction factor to Eq. (3), for example to compensate for any uncertainty in the viscosity. As discussed earlier this model does not account for surface characteristics such as roughness, elasticity, wettability and porosity all of which could account for energy loss to some extent. To investigate the effect of this factor in general on the stain size, an additional term may be incorporated into the derivation of Eq. (4). The reasonable assumption that the energy loss will depend on stain area leads to the simplest form of expression since it means that an empirical term such as BD^2 needs to be included where B is an arbitrary constant. Consequently Eq. (1) becomes:

$$\frac{1}{2}\left(\frac{\pi\rho d^3}{6}\right)v^2 + \pi\gamma d^2 = BD^2 + \frac{\pi\gamma D^2}{4}(1-\cos\theta_a) + \frac{\pi}{3\sqrt{Re}}\rho v^2 dD^2$$

Since this already contains the term dependant on D^2 describing the surface energy associated with advancing contact angle, the first two terms on the RHS may be combined into a single term represented by the constant term A in the consequent revised version of Eq. (4) as:

$$(We+12)\beta = 8 + \beta^3\left(A + \frac{4}{\sqrt{Re}}We\right) \quad (15)$$

Table 2
Examples of liquid droplet diameters used by other workers.

Reference	Droplet diameters (mm)	Liquid
[2]	~1.5	n-Heptane
[3]	2.05	Water; water + surfactant
[11]	0.55, 1.30	Water
[4]	3.0, 3.7, 4.3	Blood
[5]	2.5, 2.7, 3.6	Water; formamide
This work	3.28, 4.21, 5.15	Blood

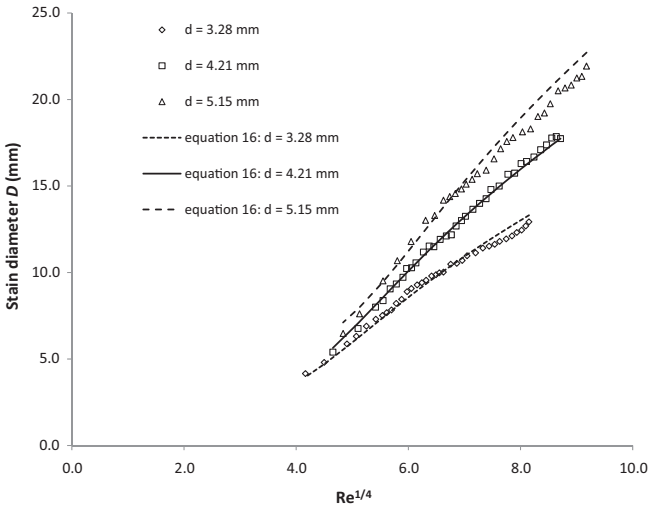

Fig. 14. Comparison of experimental data with the revised model for stain diameter.

Here A will have a minimum value of 2.6 (assuming $\theta_e = 82°$) corresponding to $B = 0$ which may then increase as additional energy is lost due to surface-specific properties. This equation may be readily evaluated to yield β using the iterative form:

$$\beta = \frac{D}{d} = \left(\frac{We + 12 - (8/\beta)}{A + 4(We/\sqrt{Re})}\right)^{1/2} \quad (16)$$

By taking the experimental value of D as an initial estimate, this converged quickly to a constant, predicted value of β in two iterations. The magnitude of A was varied until best agreement was obtained with the experimental data according to the minimisation of the sum of the squares of the residual differences criterion. The results of this calculation are given in Fig. 14.

The overall agreement of this model with the experimental measurement of stain diameter is very good over the very wide impact velocity range shown here and appears best for the data from the medium-sized droplet. The suspected discontinuity mentioned earlier that coincides with the onset of scallops around the stain is not, of course, built into this simple model and so is not reproduced though it is likely to involve a small step change in the energy dissipation. The best-fit values for A were found to be 7.6, 9.0 and 12.6 for the small, medium and large droplets respectively which reflects some dependency on droplet size. Further refinement of this model is possible but would need to be validated across measurements from a wide range of types of surface in order to properly account for the surface properties discussed previously.

5.2. Splashing behaviour on perpendicular impact

These results show that the accepted expression for splashing threshold (Eq. (6)) appears to correlate well with the formation of spines for bloodstains on paper and may be used to estimate a lower or upper limit on impact conditions for an individual stain. Although there appear to be different thresholds governing the formation of scallops and of spines and we would argue that these are distinct though related features, this differentiation does not appear to have been discussed in the literature. Indeed confusion over which feature was being referred to may have led to apparent discrepancies in splashing thresholds between some authors. Further to this, Eq. (7), with a small adjustment to the scaling factor, appears to provide a good explanation for the number of spines/scallops observed around a stain as long as the impact Weber number is below ~1000, corresponding to an impact velocity of ~4 m s^{-1} or a drop height of ~0.8 m for a droplet of

diameter 4.21 mm. Above this value this formula gives an overestimate as the length per spine around the circumference seems to approach a limiting value. This may be due to closely spaced spines being energetically unfavourable on account of the consequent high curvature of the liquid edge between them. This work shows that this limit depends to some extent on droplet size, with smaller droplets having a lower limit, though it is likely that it will be affected also by surface characteristics.

These observations on both the spreading and spine formation in circular stains imply that there are quite significant lower and upper limits on the validity of the method of determining both droplet volume and impact velocity through the simultaneous solution of Eqs. (3) and (7) [11].

5.3. Spreading behaviour for non-perpendicular impact

The stain areas have been calculated using the experimental data to enable comparison between those for angular impact and those for perpendicular impact with the same impact speed. It has been suggested [20] that the area remains unchanged as the angle decreases from 90° and the speed remains constant. However it is not clear whether these authors have provided a proper theoretical basis for this and taken account of the effect of the curvature of the elliptical stain in calculating the viscous dissipation energy term in Eq. (1) prior to using it to evaluate area. The stain area has also been used previously in the empirical investigation of angular impact data [19].

The areas measured in this current work are presented for comparison in Fig. 15. The perpendicular and non-perpendicular areas are certainly in excellent agreement for stains up to around 135 mm^2 but thereafter there is some additional spreading of up to 10% in those due to non-perpendicular impact. These larger stains correspond to drop heights above 0.3 m (impact velocities above $\sim$2.4 m s^{-1}). What is most unexpected is that there appears to be no obvious angular dependence to the comparison of these stain areas since the scatter of points for those at the lowest impact angles intermix with those from much higher angles. It was noted earlier from Fig. 9 that stain widths for those lowest angles are less than predicted theoretically so for the areas to increase in these cases, the stain lengths must show some increase over what is expected. Further, all stains at 20° impact and many at 30° and 40° have a cast-forward feature, yet the consequent loss of blood does not seem to affect the elliptical area of the stain itself to any significant extent.

The derivation of Eq. (8) is based on simple geometrical principles which assume the spreading is proportional to the geometric profile of the droplet on impact at a particular angle. For angles of 40° and above we have shown that the transverse spreading is explained only by the perpendicular velocity component. This however is the only definitive outcome as both the results for the stain aspect ratio (Fig. 10) and stain area (Fig. 15) reveal small but systematic discrepancies from the basic relationships. These suggest that there is a need for the development of a model for the spreading of elliptical stains analogous to that for circular stains (Eq. (2)).

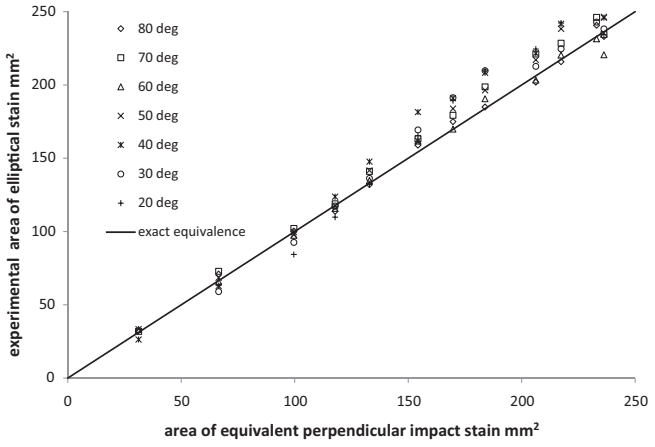

Fig. 15. Comparison of experimental stain areas for non-perpendicular and perpendicular impact at the same speed.

5.4. Splashing behaviour for non-perpendicular impact

Although this is the more complex aspect to understand, it is potentially the most useful for interpretation. Figs. 11 and 13 provide a semi-quantitative picture of the factors affecting the formation of the splash and other features observed around these stains while Fig. 12 shows that there is some theoretical basis to the angular dependence of spine formations despite the difficulty in some instances in the practical counting of these features. Indeed this is likely to be a key limiting factor in using the pattern of spines around the perimeter to interpret elliptical stains. Nevertheless, theoretical work to develop a model for the angular distribution of spines around a stain as a function of impact velocity and droplet size, as an extension to the derivation [17] of Eq. (11), remains to be done. This should include study of the transition from classic spine/scallop formation to the generation of the cast-forward feature at low velocity and low impact angles which is likely to prove most useful to case-work interpretation.

5.5. A strategy for the interpretation of single bloodstains

Finally, it is useful to consider the implications of this work for the interpretation of a single bloodstain, in particular whether the droplet volume and impact velocity may be deduced, and also what limitations and issues remain to be investigated. Despite the fact that these models for spreading and splashing have been investigated, developed and validated for stain formation on a paper substrate, they do provide some generic implications for the application and range of validity of such approaches to the interpretation of stains in general.

Initial inspection should look for suppression of spines along part of the circumference which would indicate the impact angle was not perpendicular and facilitate measurement of the length and breadth of the stain. For perpendicular impact, determination of $\pi D/N$ coupled with Fig. 8 will show whether the measurements lie in the region of validity of Eq. (7) or not. If $\pi D/N$ lies in the constant region then this strong correlation between spreading and the number of spines appears to preclude calculation of d and v from the data. However, Fig. 8 indicates some dependence on droplet size which may enable estimation of d directly. For $\pi D/N$ below this range, Eq. (7) is valid (with an appropriate constant multiplicative factor). Where spines or scallops are visible then the stain diameter is given approximately by Eq. (3) or more accurately by Eq. (16), particularly if the droplet size is large, and hence by combining these measurements d and v may be calculated.

If no scallops or spines are observed on the stain then Eq. (6) will set an upper limit on $WeRe^{1/2}$ and it is essential that Eq. (16) is used to interpret the diameter. These measurements could allow for the calculation of limiting estimates only, for d and v.

For non-perpendicular impact determination of the impact angle from stain dimensions may be followed using the conventional formula (Eq. (8)). Bearing in mind the difficulty in reliably counting spines from such stains, combining such information with Eq. (14) and the interpretation of the stain width using Eq. (10) would enable the calculation of d and v. It is suggested that this approach is more reliable than using stain area as previously suggested [19] though the accuracy may be limited

for low impact angles. For elliptical stains where no spines are present, comparison with a "splash map" such as Fig. 11 may indicate the range of the impact velocity though further work is needed to validate whether this approach is independent of droplet size i.e. can such a diagram be produced in terms of components of $WeRe^{1/2}$ say, rather than the velocity only? Combining this information with stain breadth interpreted using Eq. (10) may enable estimates of d and v to be obtained.

These comments are predicated on a proper understanding on how the fundamental equations need to be modified to account for the surface properties of a wider range of substrates such as those that might be found routinely in casework. Such surfaces may exhibit different characteristics of roughness, elasticity, wettability and porosity, and systematic studies of the effect of such properties on the spreading and splashing of blood remain to be done.

6. Conclusions

From a review of the literature and the analysis of the experimental work described in this article on the spreading and splashing of blood droplets on paper surfaces, it has been concluded that there are fundamental mathematical expressions that may form the basis of more detailed modelling of such stains. These enable us to understand the characteristics of bloodstains according to the principles of physics and mathematics thereby putting the interpretation of bloodstain patterns on a sound theoretical basis. For perpendicular impact it has been shown that the interpretation of a single stain may yield useful information on its impact conditions, though only within a very limited range of velocities would calculation of the droplet size and impact speed be achievable to a good degree of accuracy. For non-perpendicular impact, current models are more approximate and a rigorous theoretical examination of such systems remains to be done. Nevertheless, for elliptical stains similar outcomes may be obtained by using the stain width and an estimate of the number of spines but again this would be over a limited range of speeds and angles. Further, theoretical work to explain the mechanism for the formation of the cast-forward feature on low angle, low velocity impact stains would be of significant benefit to interpretation. Finally, systematic, quantitative studies of the relationships between surface properties and bloodstain characteristics are an essential prerequisite to completing our fundamental understanding of this important area of forensic science.

References

[1] M. Rein, Phenomena of liquid drop impact on solid and liquid surfaces, Fluid Dyn. Res. 12 (1993) 61–93.
[2] S. Chandra, C.T. Avedisian, On the collision of a droplet with a solid surface, Proc. R. Soc. Lond. A 432 (1991) 13–41.
[3] M. Pasandideh-Fard, Y.M. Qiao, S. Chandra, J. Mostaghimi, Capillary effects during impact on a solid surface, Phys. Fluids 8 (3) (1996) 650–659.
[4] L. Hulse-Smith, N.Z. Mehdizadeh, S. Chandra, Deducing drop size and impact velocity from circular bloodstains, J. Forensic Sci. 50 (1) (2005) 1–10.
[5] C. Ukiwe, D.Y. Kwok, On the maximum spreading diameter of impacting droplets on well-prepared solid surfaces, Langmuir 21 (2005) 666–673.
[6] D.C. Vadillo, A. Soucemarianadin, C. Delattre, D.C. Roux, Dynamic contact angle effects onto the maximum drop impact spreading on solid surfaces, Phys. Fluids 21 (2009) 12202.
[7] C.D. Stow, M.G. Hadfield, An experimental investigation of fluid flow resulting from the impact of a water drop with an unyielding dry surface, Proc. R. Soc. Lond. A 373 (1981) 419–441.
[8] R.F. Allen, The role of surface tension in splashing, J. Colloid Interface Sci. 51 (2) (1975) 350–351.
[9] R. Bhola, S. Chandra, Parameters controlling solidification of molten wax droplets falling on a solid surface, J. Mater. Sci. 34 (1999) 4883–4894.
[10] N.Z. Mehdizadeh, S. Chandra, J. Mostaghimi, Formation of fingers around the edges of a drop hitting a metal plate with high velocity, J. Fluid Mech. 510 (2004) 353–373.
[11] L. Hulse-Smith, M. Illes, A blind trial evaluation of a crime scene methodology for deducing impact velocity and droplet size from circular bloodstains, J. Forensic Sci. 52 (1) (2007) 65–69.
[12] L. Xu, Liquid drop splashing on smooth, rough and textured surfaces, Phys. Rev. E 75 (2007) 056316.
[13] R.E. Pepper, L. Courbin, H.A. Stone, Splashing on elastic membranes: the importance of early time dynamics, Phys. Fluids 20 (2008) 082103.
[14] H.L. MacDonell, Credit where it's due, J. For. Ident. 61 (3) (2011) 210–221.
[15] P.A. Pizzola, S. Roth, P.R. De Forest, Blood droplet dynamics – II, J. Forensic Sci. 31 (1) (1986) 50–64.
[16] S. Sikalo, E.N. Ganic, Phenomena of droplet surface interactions, Exp. Therm. Fluid Sci. 31 (2006) 97–110.
[17] J.C. Bird, S.S.H. Tsai, H.A. Stone, Inclined to splash: triggering and inhibiting a splash with tangential velocity, New J. Phys. 11 (2009) 063017.
[18] L. Courbin, J.C. Bird, H.A. Stone, Splash and anti-splash: observation and design, Chaos 16 (2006) 041102.
[19] C. Knock, M. Davison, Predicting the position of the source of blood stains for angled impacts, J. Forensic Sci. 52 (5) (2007) 1044–1049.
[20] J. Cui, X. Chen, F. Wang, X. Gong, Z. Yu, Study of liquid droplets impact on dry inclined surface, Asia-Pac. J. Chem. Eng. 4 (2009) 643–648.
[21] M.A. Raymond, E.R. Smith, J. Liesegang, Oscillating blood droplets – implications for crime scene reconstruction, Sci. Justice 36 (3) (1996) 161–171.
[22] D.C.D. Roux, J.J. Cooper-White, Dynamics of water spreading on a glass surface, J. Colloid Interface Sci. 277 (2004) 424–436.
[23] G. Sposito, An Introduction to Classical Dynamics, Wiley, New York, 1976.
[24] J. Rosina, E. Kvasnak, D. Suta, H. Kolarova, J. Malek, L. Krajci, Temperature dependence of blood surface tension, Physiol. Res. 56 (Suppl. 1) (2007) S93–S98.
[25] M.A. Raymond, E.R. Smith, J. Liesegang, The physical properties of blood – forensic considerations, Sci. Justice 36 (3) (1996) 153–160.
[26] R.S. Rosenson, A. McCormick, E.F. Uretz, Distribution of blood viscosity values and biochemical correlates in healthy adults, Clin. Chem. 42 (8) (1996) 1189–1195.